IEEE Access
Multidisciplinary | Rapid Review | Open Access Journal

Date of publication xxxx 00, 0000, date of current version xxxx 00, 0000.

Digital Object Identifier 10.1109/ACCESS.2017.Doi Number

Millimeter-Wave Dual-Polarized Dielectric Resonator Reflectarray Fabricated by 3D Printing with High Relative Permittivity Material

Yu-Xiang Sun[1, 2], (Member, IEEE), Di Wu[1], (Member, IEEE), and Jian Ren[3], (Member, IEEE)

[1]College of Electronics and Information Engineering, Shenzhen University, Shenzhen 518060, China.
[2]State Key Laboratory of Millimeter Waves, Southeast University, Nanjing 210096, China
[3]National Key Laboratory of Antennas and Microwave Technology, Xidian University, Xi'an, Shaanxi 710071, China

Corresponding author: Jian Ren (e-mail: renjian@xidian.edu.cn).

This work was supported in part by the National Natural Science Foundation of China under Grants 62001306, 61901316, and 61901272, in part by the Guangdong Basic and Basic Applied Research Foundation under Grant 2021A1515011323, in part by the Natural Science Foundation of SZU under Grants 2019008 and 2019010, and in part by the Open Project of the State Key Laboratory of Millimeter Waves, Southeast University, under Grant K202110.

ABSTRACT For the first time, a millimeter-wave dual-polarized dielectric resonator (DR) reflectarray fabricated by three-dimensional (3D) printing with high relative permittivity materials is presented. The unit cell of the reflectarray is composed of two elliptical DRs orthogonally placed in the center. A base layer of dielectric slab at the bottom of the unit cell is for fixture and connection with its adjacent elements. For each polarization, only the length of the long axis of one elliptical DR is varied independently to obtain the required reflecting phase response. Due to the orthogonality, high isolation and design independence between the two polarizations can be also obtained. A dual-polarized square DR reflectarray with 16 × 16 elements working in the Ka-band was designed, printed, and measured for demonstration. A measured peak antenna gain of 22.53 dBi was obtained, achieving a gain enhancement of 7.43 dB as compared with that of the feed horn.

INDEX TERMS Dual polarization, three-dimensional printing, dielectric antenna, reflectarray, high-gain antenna.

I. INTRODUCTION

Reflectarrays are a kind of high-gain antennas that can be applied to a wideband frequency range from the microwave, millimeter-wave all along to the terahertz band [1]–[7]. The unit cells with different sizes are distributed to compensate for the path differences from the focal point to each unit. When illuminated by a feeding source, the reflectarray transforms the spherical wave-front to the planar one and high directivity is obtained eventually. Compared with the traditional high-gain antennas, such as the parabolic reflector antenna or the phased array antenna, the reflectarray does not need the bulky metallic reflector or the phasing and feeding networks, which makes it compact, light-weighted, and low-cost [1], [2].

Microstrip reflectarrays are very popular high-gain antennas at the microwave band as they have low profiles and simple structures. They are usually realized in a single piece of substrate using low-cost printed-circuit-board (PCB) fabrication. However, at the millimeter-wave or higher frequency bands, microstrip reflectarrays may encounter metallic and ohmic losses, which would deteriorate the performance. The applications of dielectric resonator (DR) reflectarrays arise at the millimeter-wave frequency band and above because they have no such losses [8]–[12]. Different methods have been employed to fabricate the DR reflectarrays at the millimeter-wave bands. The traditional method is to use the computer numerical control (CNC) machining to fabricate each unit cell and then to assemble them one by one [10]. Due to the small size of the unit cell, it would be very difficult to fix all the elements accurately. Another method is by using PCB drilling on a dielectric substrate [11]–[13]. This method is preferably limited to low dielectric constant materials. For high dielectric constant substrates, the cost of high-frequency low-loss laminated substrates is very high for mass production [14].

This article has been accepted for publication in a future issue of this journal, but has not been fully edited. Content may change prior to final publication. Citation information: DOI 10.1109/ACCESS.2021.3098982, IEEE Access

With the fast prototyping capability of irregular shapes, three-dimensional (3D) printing has been used for fabricating DR reflectarrays in recent years [15]–[18]. [15] and [17] both proposed 3D printed dielectric reflectarrays with variable height elements at sub-millimeter-waves. By using the acrylonitrile butadiene styrene (ABS) material, a 3D-printed dielectric reflectarray with variable width unit cells was designed in [16]. In [18], a polarization-reconfigurable reflectarray was realized by 3D printing for 5G millimeter-wave applications. All these designs are also limited to low relative permittivity materials (ε_r < 4.4) and therefore resulting in a large size or non-planar configuration. Several 3D printing designs with high relative permittivity materials (ε_r: 9.8~10) were reported [19]–[23]. Wideband end-fire dielectric antenna and omnidirectional dielectric resonator antenna (DRA) fabricated by 3D printing are studied in [22] and [23], respectively. In [19], a wideband circularly polarized dielectric reflectarray consisting of cross-shaped elements at Ka-band fabricated by 3D printing is proposed. Another Ka-band 3D printed dielectric reflectarray for generating orbital angular momentum (OAM) beams is investigated in [20]. However, they are usually operated in the microwave range [22]–[23] or with a single polarization or function [21].

In this paper, a millimeter-wave DR reflectarray with dual-polarized operation fabricated by 3D printing with high relative permittivity material is presented. The dual polarizations are realized by using two elliptical DRs which are arranged in an orthogonal manner. By only changing the long axis length of each DR, the required reflecting phase range for reflectarray design is obtained. Due to the orthogonality of the two DRs, high isolation and design independence between the two polarizations can be also obtained. The collimated beam direction of each polarized reflectarray can be designed independently and almost arbitrarily. Working in the frequency range from 30 GHz to 40 GHz, a 256-element dual-polarized DR reflectarray is printed using a high dielectric constant material of 10. Measurement was carried out for verification and good agreement between the measured and simulated results is obtained.

II. DUAL-POLARIZED UNIT CELL DESIGN

Figure 1(a) shows the configuration of the unit cell of the dual-polarized DR reflectarray. The square unit cell has two elliptical DRs orthogonally placed at the center. The side length (periodicity) of the unit cell is L_0. Below the elliptical DRs is a square dielectric base, which is fully backed by a copper ground plane for the reflection of incident waves. The short and long axis of the x-directed elliptical DR are defined as l_1 and k_1l_1, respectively, and they are l_2 and k_2l_2 for the y-directed elliptical DR. It is noted that l_1 and l_2 are fixed whereas the ratios k_1 and k_2 can be varied independently. Therefore, the sizes of the two elliptical DRs can be only determined by the ratios k_1 and k_2. Thicknesses of the elliptical DRs and the base are given as h and h_1, respectively. The dielectric material used for the elliptical DRs and the base has a dielectric constant of ε_r. The parameter values of the unit cell and their descriptions are listed in Table I. It is worth mentioning that elliptical DRs are selected in this design for demonstration because such non-axial-symmetric shapes are not easy to be fabricated by traditional methods, such as CNC machining or PCB drilling, whereas they can be quickly prototyped by 3D printing, which shows its advantage of fast prototyping of irregular shapes. In addition, the unit cell contains two orthogonal elliptical DRs because the fields excited inside the two DRs are normal to each other so that each DR can be tuned independently. This enables and facilitates the independent design of the dual-polarized reflectarray.

The reflection phase and amplitude responses of the unit cell were studied in ANSYS HFSS [24] using the Floquet model illustrated in Fig. 1(b). The unit cell is enclosed by the periodic boundary condition (PBC), which contains two pairs of perfect electric/magnetic conductor boundaries. Floquet port was employed for excitation of the dual-polarized unit cell. The size of the elliptical DRs, namely the ratios k_1 and k_2 are varied for the required reflection phase range. In this model, the coupling between the cells has been taken into account. The model is based on the assumption that the neighboring cells are of uniform sizes. To approximate this assumption, linear response and no sudden change in the phase curve are preferred. Without considering the mutual coupling between the unit cells, the reflecting phase response obtained will be not accurate while the antenna gain of the final reflectarray will drop.

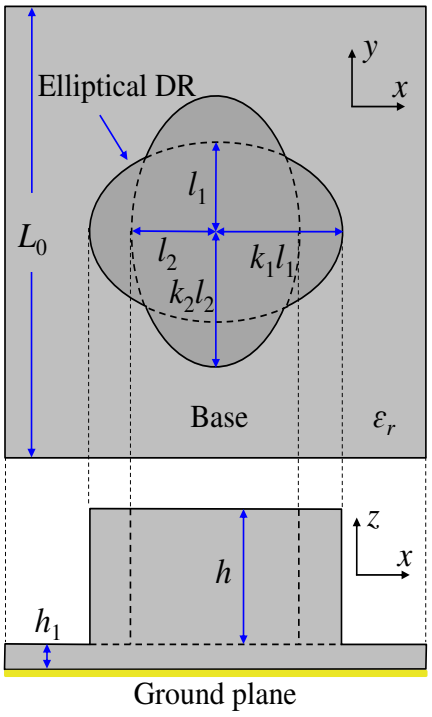

(a)

This article has been accepted for publication in a future issue of this journal, but has not been fully edited. Content may change prior to final publication. Citation information: DOI 10.1109/ACCESS.2021.3098982, IEEE Access

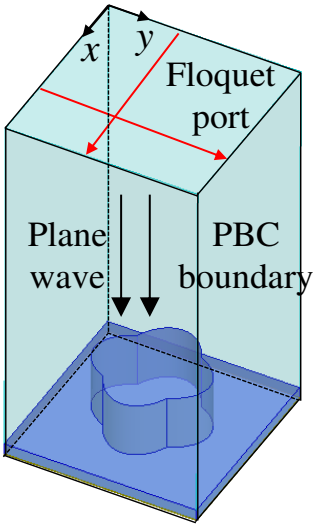

(b)

FIGURE 1. (a) Configuration of unit cell; (b) Floquet model setup in ANSYS HFSS.

TABLE I
PARAMETER VALUES OF UNIT CELL OF DR REFLECTARRAYS

Para.	Value	Description
L_0	5 mm	Side length (periodicity) of unit cell
H	1.5 mm	Height of elliptical DR
h_1	0.3 mm	Height of dielectric base
l_1	1 mm	Short axis length of x-directed elliptical DR
l_2	1 mm	Short axis length of y-directed elliptical DR
k_1	1~2.5	Ratio between long and short axis of x-directed elliptical DR
k_2	1~2.5	Ratio between long and short axis of y-directed elliptical DR

Figure 2 shows the reflection phase and amplitude responses of the unit cell under both normal and oblique incidences at the center frequency of 35 GHz. It is noted that when the size of one elliptical DR varies, the size of the other one keeps fixed. It can be found from Figure 2 that with x-polarized wave incidence and size variation of x-directed DRs, the x-polarized reflection phase range is over 360° as indicated by the black line. Whereas the y-polarized reflection phase has a narrow range of only 100° as indicated by the red dotted line. Due to the different reflection phase responses, the DR reflectarray of each polarization can be designed with much independence. Under the oblique incidences of θ = 30º or ϕ = 30º, the curves of the reflection phase are close to the one under normal incidence with small differences of below 20º, and therefore the normal incidence can be used to approximate the oblique ones in this design. It can be also found from Fig. 2 that the reflection amplitudes of the x-polarized unit cell under normal incidence are all above -0.2 dB when k_1 varies in the range from 1 to 2.5 with a step of 0.05. This indicates very low reflection loss and nearly uniform illumination over all the unit cells. Similar results can be also observed under the oblique incidences or when there are y-polarized incident waves, and therefore they are not shown here for simplicity.

Figure 3 shows the simulated E-fields distribution of the unit cell under x-polarized normal incidence at 35 GHz. It can be found that the x-directed DR was excited and its fields are much stronger than those in the y-directed one, showing good isolations and ensuring the independent tuning between the two polarizations.

The contour plot of the reflection phase of x-polarized elliptical DR for different ratios k_1 in the frequency range from 30 GHz to 40 GHz is shown in Fig. 4. No sudden change in the reflection phase is found and acceptable linearities of the reflection phase are observed. Reflection phase ranges of over 360º are obtained for most frequency points except the upper and lower regions (*i.e.* 331.3º at 30 GHz and 297.7º at 40 GHz). It was expected that the reflection phase of y-polarized elliptical DR for different ratios k_2 is the same as that of x-polarized and therefore it is again not shown here for brevity.

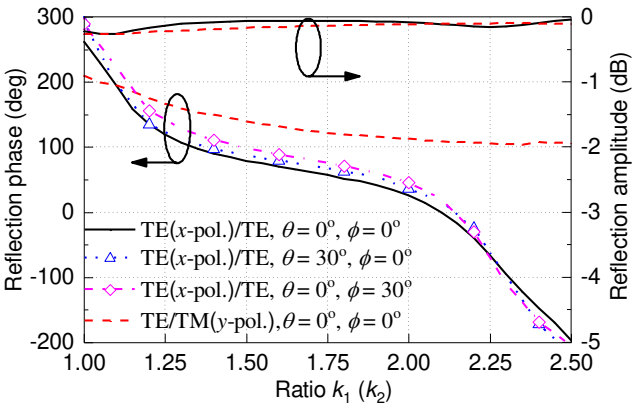

FIGURE 2. Simulated reflection phase and amplitude responses under normal and oblique incidence.

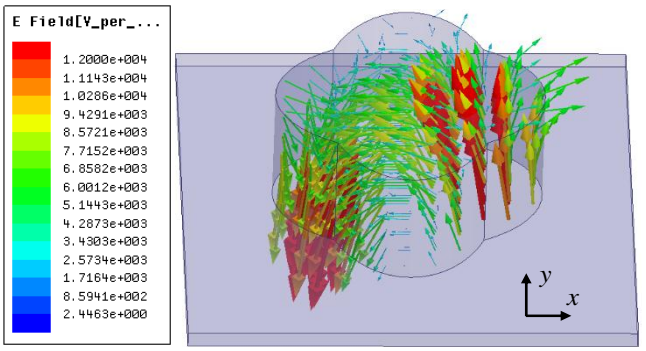

FIGURE 3. Simulated *E*-field distribution of unit cell with *x*-polarized normal incident waves.

This article has been accepted for publication in a future issue of this journal, but has not been fully edited. Content may change prior to final publication. Citation information: DOI 10.1109/ACCESS.2021.3098982, IEEE Access

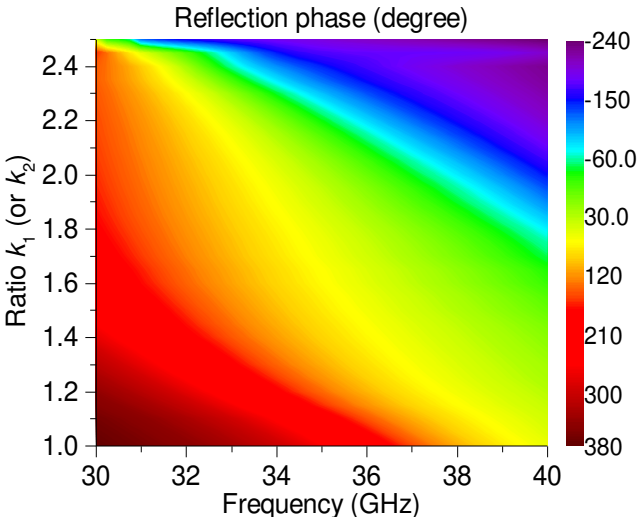

FIGURE 4. Simulated reflection phase of *x*-polarized unit cell for different ratios ($1 \le k_1$ (or k_2) ≤ 2.5) in frequency range from 30 GHz to 40 GHz.

III. DUAL-POLARIZED REFLECTARRAY DESIGN

Based on the simulated results of the unit cell, a dual-polarized square DR reflectarray consisting of 256 elements (16×16) is designed in this section.

First, the required phase compensations of all the unit cells of the two polarizations need to be calculated, by using the formula in [1]–[2]. In this design, the feed horn is placed at a distance of $d_f = 70$ mm to the center of the reflectarray. To avoid the blockage problem caused by the feed horn, there is an angular offset of 30º between the incident waves and the -z axis. Besides, to facilitate the measurement of the radiation patterns of the reflectarray in both cutting planes, its collimated mainbeam is to the boresight direction, giving $\theta_b = 0°$ in the formula. With these specifications, the required phase compensations of the x-polarized elliptical DRs over the square aperture were calculated at the center frequency 35 GHz and plotted in Fig. 5(a). For demonstration purposes and to simplify the design, the specifications of y-polarized elliptical DRs are defined the same as those of x-polarized case, and thus the calculated phase compensation distribution is also the same with respect to their feeding sources, as shown in Fig. 5(b).

In the next step, the ratios k_1 and k_2 of each x- and y-polarized elliptical DRs need to be determined. According to the required phase compensation distribution in Fig. 5 and the curve of the reflecting phase response of the unit cell in Fig. 2, the ratios k_1 of each x-polarized elliptical DRs can be matched at the center frequency 35 GHz. The ratios k_2 of y-polarized unit cells can be determined in the same way.

Finally, with known k_1 and k_2 values in each unit cell, the sizes of all the unit cells are determined. With the assistance of a MATLAB API script [14], a 16×16, 256-element dual-polarized DR reflectarray was built automatically in ANSYS HFSS. The elliptical DRs and the dielectric base are modeled separately and merged in the software. In the meanwhile, the material properties were also assigned.

To summarize the design process of the dual-polarized DR reflectarray, some design guidelines are given here:

(a). Choose a proper dual-polarized DR unit cell structure that each polarization can be designed and tuned independently. Obtain its reflecting phase response as a function of a certain parameter under both normal and oblique incidences for different frequencies by using the Floquet model.

(b). Taking the design specifications into account, calculate the phase compensation of each unit cell in the DR reflectarray aperture.

(c). According to the reflecting phase response curve, match the required phase compensation with the varying parameter and determine the size of each unit cell of each polarization.

(d). Together with the feed horns, build the whole DR reflectarray model and finalize the results.

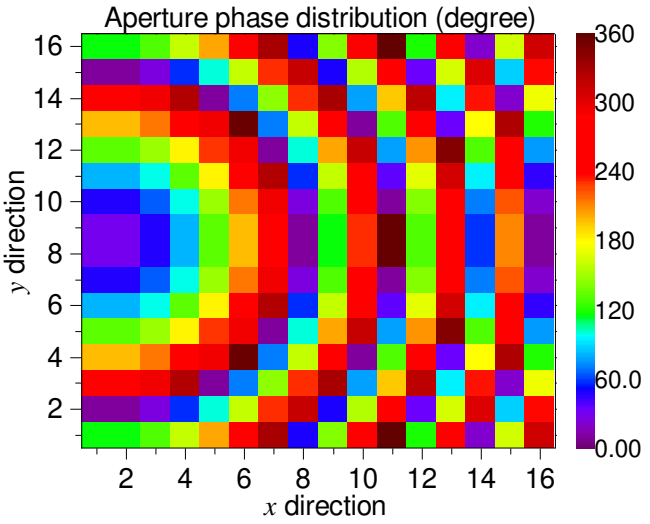

(a)

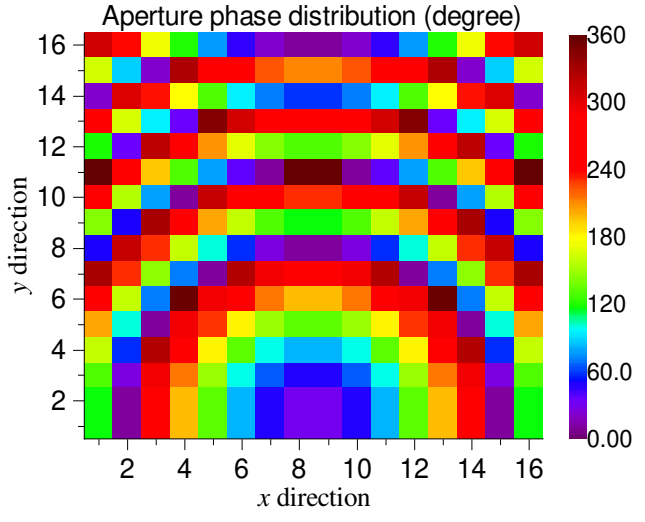

(b)

This article has been accepted for publication in a future issue of this journal, but has not been fully edited. Content may change prior to final publication. Citation information: DOI 10.1109/ACCESS.2021.3098982, IEEE Access

FIGURE 5. Calculated compensation phase distribution over square aperture of DR reflectarray at center frequency 35 GHz: (a) *x*-polarized; (b) *y*-polarized.

IV. SIMULATED AND MEASURED RESULTS

The dual-polarized DR reflectarray was simulated together with two feed horns [25] in ANSYS HFSS. In this design, two identical circular horns were employed for illumination of the dual-polarized dielectric reflectarray. The measured and simulated S-parameters of the feed horns were studied. The measured and simulated -10-dB impedance bandwidths can generally cover the whole frequency range from 30 GHz to 40 GHz, although the measured reflection coefficients are slightly above -10 dB at 30.95 GHz (-8.81 dB), 37.90 GHz (-9.44 dB), and 39.65 (-8.52 dB). Both measured and simulated isolations between the two horns are generally over 30 dB. Radiation patterns of the feed horn at 35 GHz were also studied. It was found that in the angular range of $-30^{\circ} \le \theta \le 30^{\circ}$, the amplitudes in the two principal planes are almost overlapped with small differences. The antenna gain at 35 GHz was found as 14.7 dBi. Within the frequency range of interest, antenna gains of 12.5 to 15.1 dBi were also obtained.

By using 3D printing, the dual-polarized DR reflectarray was fabricated. It was printed by a Creator Pro Flashforce 3D printer with a commercial filament of PREPERM 3-D ABS DK 10.0 from Premix [26]. The filament has a high dielectric constant of ε_r = 10, loss tangent of tan δ = 0.003. It took about one hour and 40 minutes to print the reflectarray at a nozzle and a platform temperature of 235 °C and 105 °C, respectively. For facilitating the measurement, a dielectric supportor (ε_{rs} = 2.1) was also printed to hold the feed horns and to accommodate the reflectarray. The whole simulated model of the proposed DR reflectarray consisting of the 3D printed reflectarray, 3D printed supportor and the feed horns are shown in Fig. 6(a), and photos of the reflectarray prototype and the fabricated reflectarray are shown in Fig. 6(b) and (c), respectively. It is noted that in each unit cell, the sizes of *x*- and *y*-directed elliptical DRs may vary. For some unit cells in the prototype in Fig. 6(c), there may be some special shapes. For example, when it is formed by a very small *x*-directed elliptical DR (k_1 is small, close to 1) and a large *y*-directed DR (k_2 is large, close to 2.5). In this case, we can only see the *y*-directed DR and the *x*-directed is included in the *y*-directed one, and vice versa. Another case is when the sizes of *x*-and *y*-directed elliptical DRs are both not very large and equal or very close to each other (k_1 equals to k_2), we may see a circle in the top view due to the printing resolution.

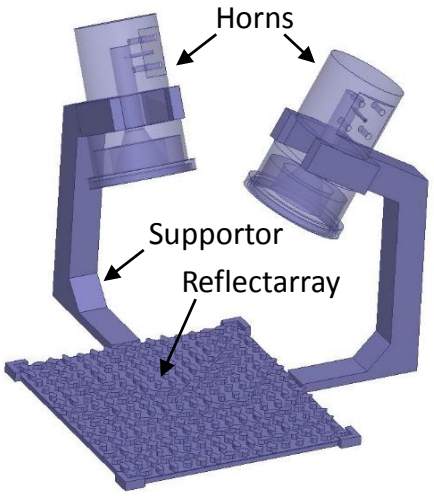

(a)

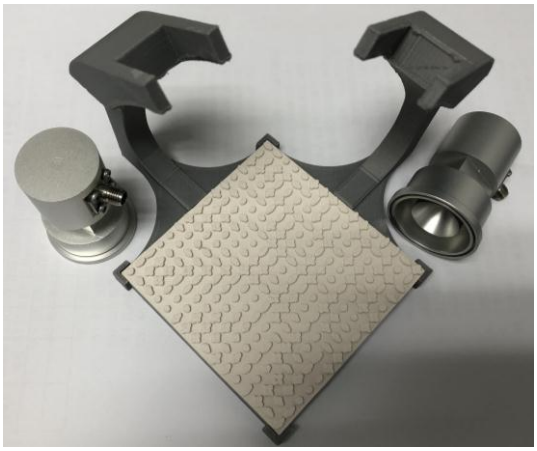

(b)

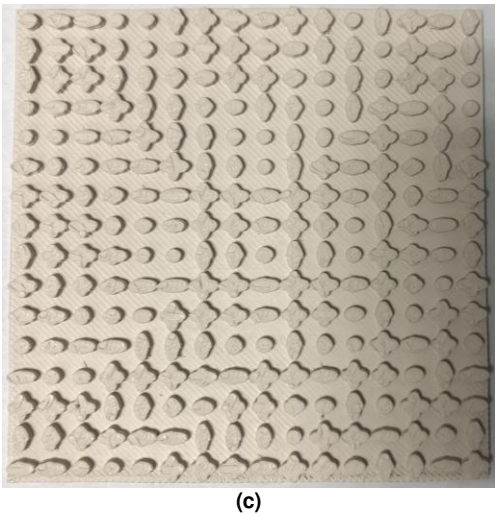

(c)

FIGURE 6. (a) Whole simulated model of 3D-printed dual-polarized DR reflectarray; (b) Fabricated prototype including the dual-polarized DR reflectarray, supportor, and feed horns; (c) Top view of 3D-printed dual-polarized DR reflectarray.

The dual-polarized DR reflectarray was measured. The S-parameters were measured using a vector network analyzer

This article has been accepted for publication in a future issue of this journal, but has not been fully edited. Content may change prior to final publication. Citation information: DOI 10.1109/ACCESS.2021.3098982, IEEE Access

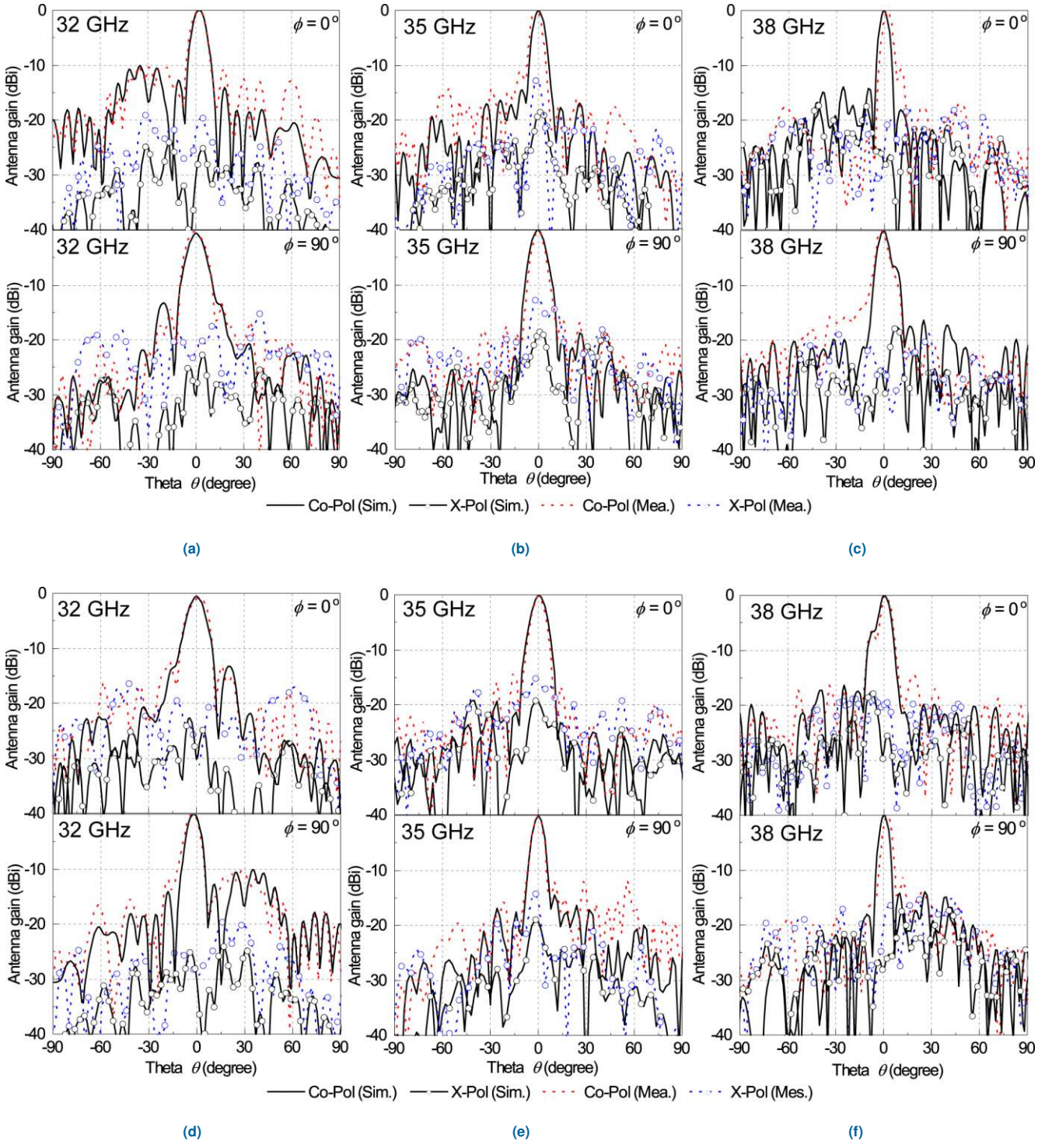

FIGURE 7. Measured and simulated normalized radiation patterns of dual-polarized DR reflectarray. (a) *x*-polarized at 32 GHz in planes of ϕ = 0° and 90°. (b) *x*-polarized at 35 GHz in planes of ϕ = 0° and 90°. (c) *x*-polarized at 38 GHz in planes of ϕ = 0° and 90°. (d) *y*-polarized at 32 GHz in planes of ϕ = 0° and 90°. (e) *y*-polarized at 35 GHz in planes of ϕ = 0° and 90°. (f) *y*-polarized at 38 GHz in planes of ϕ = 0° and 90°.

Keysight E8361A with the existence of the DR reflectarray and the dielectric supportor, whereas the radiation pattern and antenna gain were measured by an indoor far-field test range. In particular, the antenna gain was obtained by using the comparison method with a standard gain horn. When one port is measured, the other port is terminated with a 50-Ω load.

The measured and simulated radiation patterns of the DR reflectarray at 32 GHz, 35 GHz and 38 GHz are shown in Fig. 7. Good agreement between the measured and simulated

This article has been accepted for publication in a future issue of this journal, but has not been fully edited. Content may change prior to final publication. Citation information: DOI 10.1109/ACCESS.2021.3098982, IEEE Access

TABLE II
COMPARISON BETWEEN OUR DESIGN WITH PREVIOUS 3D-PRINTED MM-WAVE REFLECTARRAYS

Ref.	Fabrication method	Center freq. f_0	ε_r	No. of unit cells	Physical aperture (mm^2)	Height (mm)	Gain enhanced /peak gain	Aperture Efficiency	Remarks
[13]	Monolithic	31 GHz	10	576	120×120 $12.4\lambda_0\times12.4\lambda_0$	0.8 $0.082\lambda_0$	8.3 dB 28.28 dBi	34.8%	Single pol., medium cost
[14]	PCB drilling	35 GHz	10.2	446	$\pi\times60\times60$ $\pi\times7\lambda_0\times7\lambda_0$	1.27 $0.148\lambda_0$	9.2 dB 23.9 dBi	12.7%	Single pol., high cost
[15]	3D printing	100 GHz	2.78	400	30×30 $10\lambda_0\times10\lambda_0$	2.32 $0.77\lambda_0$	6.9 dB 18.9 dBi	6.18% ~15.5%	Single pol.
[16]	3D printing	30 GHz	4.4	625	120×120 $12.5\lambda_0\times12.5\lambda_0$	4.7 $0.63\lambda_0$	9.0 dB 28 dBi	34.9%	Single pol.
[17]	3D printing	220 GHz	2.64	1600	28×28 $20.5\lambda_0\times20.5\lambda_0$	1.7 $1.25\lambda_0$	3.6dB 27.4 dBi	10.38%	Single pol.
[19]	3D printing	30 GHz	9.8	225	112.5×112.5 $11.25\lambda_0\times11.25\lambda_0$	5.725 $0.573\lambda_0$	N.A. 24.2dBi	16.5%	Circular pol.
[20]	3D printing	30 GHz	10	400	100×100 $10\lambda_0\times10\lambda_0$	6 $0.6\lambda_0$	N.A. 20.4 dBi	8.73%	OAM generation
[27]	3D printing	60 GHz	2.7	512	54.4×54.4 $10.88\lambda_0\times10.88\lambda_0$	9 $1.8\lambda_0$	N.A. 27.9dBi	40.5%	Filtering, metal coating
[28]	3D printing	65GHz/ 24 GHz	2.5/4	484/100	77×77 $16.68\lambda_0\times16.68\lambda_0$ $/6.16\lambda_0\times6.16\lambda_0$	29.3 6.35/2.34 λ_0	10.7/2.15 dB 30.7/23.2 dBi	33.6% /43.8%	Multilayer, high profile single pol.
This work	3D printing	35 GHz	10	256	80×80 $9.33\lambda_0\times9.33\lambda_0$	1.8 $0.21\lambda_0$	7.4 dB 22.53 dBi	16.4%	Dual-pol, independent design

λ_0 is the wavelength in air at center frequency f_0.

mainbeams can be observed. Due to the imperfect printing and measurement setup, the measured sidelobes become deteriorated, but for the *x*-polarization, they are still below (-10.2 dB, -14.2 dB), (-14.1 dB, -16.7 dB) and (-17.0 dB, -15.6 dB) in the planes of ϕ = (0°, 90°) at 32 GHz, 35 GHz and 38 GHz, respectively. For the *y*-polarization case, similar results of (-13.1 dB, -10.1 dB), (-16.6 dB, -11.8 dB) and (-11.2 dB, -14.4 dB) are also obtained. At the center frequency of 35 GHz, both the measured and simulated cross-polarized fields at each polarization are generally around -20 dB, showing good polarization purity.

Measured and simulated antenna gains of the dual-polarized reflectarray in the boresight direction (θ = 0°) are shown in Fig. 8 and reasonable agreement can be observed. With reference to the figure. Both in the simulation and measurement, the results of the *x*-polarized are very close to those of the *y*-polarized, showing good consistency. A measured peak antenna gain of 22.53 dBi is observed at 36 GHz. Compared with the feed horn, a gain enhancement of 7.43 dB is achieved. It is noted that the difference between the measured and simulated results can be attributed to the printing tolerance and rough surface.

A comparison between our reflectarray and some previous millimeter-wave dielectric reflectarrays is conducted in Table II. Previous fabrication methods, such as monolithic [13] or PCB drilling [14] use high relative permittivity materials and can have compact footprints or very low profiles (0.082 λ_0 in [13] and 0.148 λ_0 in [14]). However, for the PCB drilling method [14], the choice of the substrate thickness is very limited, and the cost of high-frequency low-loss laminated substrates for millimeter-wave applications could be very high. 3D printing method is very popular for fabricating dielectric reflectarrays at millimeter-wave bands or beyond. It can provide high flexibility in choosing the thicknesses or heights of the unit cells and the fabrication cost could be much lower. It also provides fast prototyping capability of irregular shapes. Most reported 3D-printed designs employ relative permittivity materials of ε_r < 4.4 [16, 19, 20, 28], most of which are below 3 [15, 17, 27]. With reference to the table, using low relative permittivity materials usually leads to high profiles of over $0.573\lambda_0$ [15–17, 19, 20]. The heights of [27, 28] are even larger than $2\lambda_0$, to the scale of over $6\lambda_0$. Our 3D-printed design, using high relative permittivity materials of ε_r = 10, has a low profile of only $0.21\lambda_0$. In terms of aperture efficiency, most millimeter-wave reflectarray designs are in the range of below 20% [14, 17, 19] or even below 10% [15, 20], and some high-efficiency designs can be over 33.6% [13, 16, 27, 28]. Our design, with a value of 16.4%, is in the middle place. Another remarkable point we need to take into account in the comparison is that except [29] for a dual-band design at the sacrifice of high profile, all the other previous designs can only realize a single polarization or single function (OAM generation [20], spatial filtering [27]), whereas our 3D-printed design realizes dual polarizations with independent control, which excels the previous designs.

To sum up, by making use of high relative permittivity materials, our 3D-printed DR reflectarray, has a low profile, an acceptable medium aperture efficiency, and realizes dual independently-tuned polarizations, which is a promising low-cost candidate for high-gain dual-polarized millimeter-wave applications.

This article has been accepted for publication in a future issue of this journal, but has not been fully edited. Content may change prior to final publication. Citation information: DOI 10.1109/ACCESS.2021.3098982, IEEE Access

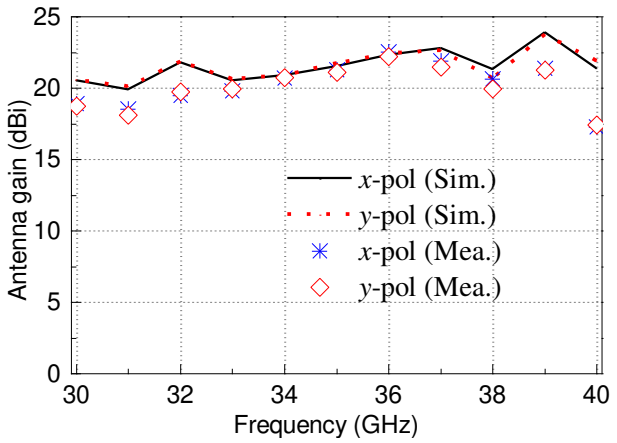

FIGURE 8. Measured and simulated antenna gain of dual-polarized DR reflectarray in boresight direction (θ = 0°).

IV. CONCLUSION

A 3D-printed millimeter-wave dual-polarized DR reflectarray has been investigated in this letter. A cross-shaped unit cell containing two orthogonal elliptical DRs has been employed to obtain the required phase responses along the *x*- and *y*-polarizations. It has been studied that varying the size of one elliptical DR does not affect the reflected phase of another orthogonal DR, which facilitates the independent design of the reflectarray.

By using 3D printing technology, for demonstration, a 256-element square dual-polarized DR reflectarray working in the frequency range of 30 GHz to 40 GHz has been printed and measured. The measured peak antenna gain of 22.53 dBi has been obtained. It is noted that in this design although the collimated mainbeams of both polarizations point to the boresight, they can be designed to other values independently.

REFERENCES

[1] J. Huang and J. A. Encinar, *Reflectarray Antennas*, New Jersey, USA: John Wiley & Sons, 2008.

[2] P. Nayeri, F. Yang, and A. Z. Elsherbeni, *Reflectarray Antennas: Theory, Designs, and Applications*. Hoboken, NJ, USA: Wiley, 2018.

[3] D. M. Pozar, S. D. Targonski, and H. D. Syrigos, "Design of millimeter wave microstrip reflectarrays," *IEEE Trans. Antennas Propag.*, vol. 45, no. 2, pp. 287–296, Feb. 1997.

[4] S.-W. Qu, H. Yi, B. J. Chen, K. B. Ng, and C. H. Chan, "Terahertz refecting and transmitting metasurfaces," *Proc. IEEE*, vol. 105, no. 6, pp. 1166–1184, Jun. 2017.

[5] H. Yi, S.-W. Qu, K.-B. Ng, C. K. Wong, and C. H. Chan, "Terahertz wavefront control on both sides of the cascaded metasurfaces," *IEEE Trans. Antennas Propag.*, vol. 66, no. 1, pp. 209–216, Jan. 2018.

[6] H. Xin and M. Liang, "3-D-printed microwave and THz devices using polymer jetting techniques," *Proc. IEEE*, vol. 105, no. 4, pp. 737–755, Apr. 2017.

[7] B. Zhang, Y. Guo, H. Zirath, and Y. P. Zhang, "Investigation on 3-D-printing technologies for millimeter-wave and terahertz applications," *Proc. IEEE*, vol. 105, no. 4, pp. 723–736, Apr. 2017.

[8] K. M. Luk and K. W. Leung, Eds., *Dielectric Resonator Antennas*, Baldock, U. K.: Research Studies Press, 2003.

[9] A. Petosa, *Dielectric Resonator Antenna Handbook*, Norwood, MA, USA: Artech House, 2007.

[10] M. G. Keller, J. Shaker, A. Petosa, A. Ittipiboon, M. Cuhaci, and Y. M. M. Antar, "A Ka-band dielectric resonator antenna reflectarray," *30th European Microw. Conf.*, pp. 1–4, 2000.

[11] M. Moeini-Fard and M. Khalaj-Amirhosseini, "Inhomogeneous perforated reflect-array antennas," *Wireless Engineering Technol.*, vol. 2, pp. 80–86, 2011.

[12] M. K. T. Al-Nuaimi and W. Hong, "Discrete dielectric reflectarray and lens for E-band with different feed," *IEEE Antennas Wireless Propag. Lett.*, vol. 13, pp. 947–950, 2014.

[13] M. H. Jamaluddin, *et al.*, "Design, fabrication and characterization of a dielectric resonator antenna reflectarray in Ka-band," *Progress Electromag. Research B*, vol. 25, pp. 261–275, 2010.

[14] Y.-X. Sun and K. W. Leung, "Millimeter-wave substrate-based dielectric reflectarray," *IEEE Antennas Wireless Propag. Lett.*, vol. 17, no. 12, pp. 2329–2333, Dec. 2018.

[15] P. Nayeri, *et al.*, "3D printed dielectric reflectarrays: low-cost high-gain antennas at sub-millimeter waves," *IEEE Trans. Antennas Propag.*, vol. 62, no. 4, pp. 2000–2008, Apr. 2014.

[16] S. Zhang, "Three-dimensional printed millimetre wave dielectric resonator reflectarray," *IET Microw. Antennas Propag.*, vol. 11, no. 14, pp. 2005–2009, 2017.

[17] M. D. Wu *et al*, "Design and measurement of a 220 GHz wideband 3-D printed dielectric reflectarray," *IEEE Antennas Wireless Propag. Lett.*, vol. 17, no. 11, pp. 2094–2098, Nov. 2018.

[18] P. Mei, S. Zhang, and G. F. Pedersen, "A wideband 3-D printed reflectarray antenna with mechanically reconfigurable polarization," *IEEE Antennas Wireless Propag. Lett.*, vol. 19, no. 10, pp. 1798–1802, Oct. 2020.

[19] B. Li, C. Y. Mei, and X. Lv, "A 3-D-printed wideband circularly polarized dielectric reflectarray of cross-shaped element," *IEEE Antennas Wireless Propag. Lett.*, vol. 19, no. 10, pp. 1734–11738, Oct. 2020.

[20] B. Li, P. F. Jing, L. Q. Sun, K. W. Leung, and X. Li, "3D printed OAM reflectarray using half-wavelength rectangular dielectric element," *IEEE Access*, vol. 8, pp. 142892–142899, 2020.

[21] Y.-X. Sun and D. Wu, "Millimeter-wave linearly-polarized dielectric reflectarray using 3D printing," in Proc. of *International Conf. Microwave Millimeter Wave Technol.*, Shanghai, China, Sep. 23–25, 2020.

[22] J. Huang, S. J. Chen, Z. Xue, W. Withayachumnankul, and C. Fumeaux, "Wideband endfire 3-D-printed dielectric antenna with designable permittivity," *IEEE Antennas Wireless Propag. Lett.*, vol. 17, no. 11, pp. 2085–2089, Nov. 2019.

[23] Z.-X. Xia, K. W. Leung, and K. Lu, "3D-printed wideband multi-ring dielectric resonator antenna," *IEEE Antennas Wireless Propag. Lett.*, vol. 18, no. 10, pp. 2110–2114, Oct. 2019.

[24] ANSYS HFSS: High Frequency Structure Simulator Based on the Finite Element Method, Ansoft Corp., Canonsburg, PA, USA, [Online]. Available: http://www.ansoft.com/

[25] M. A. Moharram and A. A. Kishk, "Optimum feeds for reflectarray antenna: synthesis and design," *IEEE Trans. Antennas Propag.*, vol. 64, no. 2, pp. 469–483, Feb. 2016.

[26] [Online]. Available: https://www.preperm.com/

[27] G.-B. Wu, Y.-S. Zeng, K. F. Chan, B.-J. Chen, S.-W. Qu, and C. H. Chan, "High-gain filtering reflectarray antenna for millimeter-wave applications," *IEEE Trans. Antennas Propag.*, vol. 68, no. 2, pp. 805–812, Feb. 2020.

[28] J. Zhu, Y. Yang, D. McGloin, S. Liao, and Q. Xue, "3-D printed all-dielectric dual-band broadband reflectarray with a large frequency-ratio," *IEEE Trans. Antennas Propag.*, 2021 (in early access).